Catalysis Today 171 (2011) 156–167

Contents lists available at ScienceDirect

Catalysis Today

journal homepage: www.elsevier.com/locate/cattod

Pt-implanted intermetallides as the catalysts for CH_4–CO_2 reforming

Larisa A. Arkatova[a,*], Oleg V. Pakhnutov[a], Alexandr N. Shmakov[b], Yury S. Naiborodenko[c], Nikolai G. Kasatsky[c]

[a] Department of Chemistry, Tomsk State University, Lenin Avenue. 36, Tomsk 634050, Russia
[b] Boreskov Institute of Catalysis, Akademika Lavrentieva Avenue 5, Novosibirsk 630090, Russia
[c] Department of Structural Macrokinetics, Tomsk Scientific Center, Siberian Branch, Russian Academy of Sciences, Academichesky Avenue 10/3, Tomsk 634021, Russia

ARTICLE INFO

Article history:
Received 6 November 2010
Received in revised form 20 January 2011
Accepted 7 March 2011
Available online 11 May 2011

Keywords:
CH_4–CO_2 reforming
Synthesis gas
Intermetallides
Self-propagating high-temperature synthesis
Ion implantation

ABSTRACT

A new type of catalytic system on the base of Ni_3Al intermetallic compound was proposed for CO_2 reforming of methane. Several catalysts were prepared by self-propagating high temperature synthesis and characterized by XRD (*in situ* and *ex situ*), DTA-TG, SEM + EDS, HRTEM + EDS and XPS. Ion implantation was used as a method of catalyst surface modification. Activity testing has been performed in the fixed bed reactor at the temperatures of 600–900 °C under atmospheric pressure and the reactant molar ratio of 1. The structure and morphology of different types of carbon deposits obtained on the surface of unmodified Ni_3Al were investigated. The results indicated that the addition of a low amount (less than 0.1 wt%) of Pt to the Ni_3Al intermetallide leads to a decrease in carbon deposition and Pt-implanted catalysts were stable for a long period of time. The evidence suggests that the differences in the stabilities may be due to the following reasons: (1) Pt prevents Ni phase sintering by avoiding particle coalescence, which is the main sintering process under severe CH_4–CO_2 reforming conditions, (2) Pt hinders deactivating carbon formation by limiting bulk nickel carbide and therefore carbon filament formation, which may lead to reactor plugging and/or particle fragmentation, and by suppressing encapsulating carbon formation which limits access of reactant to the active nickel phase.

1. Introduction

Natural gas, coal and crude oil are the basis of the modern energy supply industry, chemical industry and transportation sector [1]. The use of fossil resources results in strong liberation of CO_2 and its accumulation in our planet's atmosphere. Thus, CO_2 and released CH_4 play a major role in the global warming effect [2,3] hence the output of these gases must be reduced. Besides, the raw material prices for the above mentioned resources are increasing exponential over the recent years [1]. One contribution to reduce the greenhouse effect and a simultaneous economical utilization of fossil resources is the use of CO_2 and CH_4 as chemical feedstock [3–5]. A high promising reaction therein is the CO_2 reforming of methane; often called dry reforming of methane (DRM) wherein CO_2 and CH_4 react to synthesis gas or syngas (CO and H_2) [6–8]:

$$CH_4 + CO_2 = 2CO + 2H_2, \quad \Delta H = 247.3 \ \text{kJ mol}^{-1} \qquad (1)$$

Due to its highly endothermic property, DRM also has desirable thermodynamic characteristics of a chemical energy transmission system (CETS) [9]. Besides, this reaction plays a potentially important role in the industry as well as the steam reforming reaction, especially due to the generation of syngas with a low H_2/CO ratio that can be preferentially used for the production of valuable oxygenated chemicals and long-chain hydrocarbons [4,6]. DRM has also been suggested as a candidate for solar energy storage [5], as a method of recovering excess heat from gas turbine exhaust [6], as a source of CO and H_2 for flame stabilization in low temperature methane fired gas turbines [7] and for dimethyl ether (DME) production (in two stages) particularly. DME is excellent as a clean fuel for diesel engines compared with the light oil currently used as a diesel fuel [10–12].

CH_4–CO_2 reforming was studied by many scientists over the most VIII group transition metals (except osmium), especially noble metals and Ni based catalysts [13–18]. Nickel seems to be the most interesting metal due to its lower cost but the great challenge for Ni catalysts is that they suffer from severe catalyst deactivation due to sintering, metal oxidation, and especially significant carbon formation [4,5,13]. A great effort has been made to develop Ni-based catalysts with improved performance: lower coke deposition on the metal surface and higher stability against metal sintering. Many investigations over supported Ni catalysts have indicated that the modification of the supports with alkali- and alkaline-earth oxides, such as La-doped Ni/Al_2O_3 [19], Ni/yttria-doped ceria catalysts [20] play an important role in the catalytic activity and in

* Corresponding author. Tel.: +7 3822473449; fax: +7 3822529895.
E-mail address: larisa-arkatova@yandex.ru (L.A. Arkatova).

0920-5861/$ – see front matter © 2011 Elsevier B.V. All rights reserved.
doi:10.1016/j.cattod.2011.03.014

the coking resistance of the catalysts. Sadykov [21] developed the coke resistant fluorite-like mixed oxides promoted by Pt for DRM. The addition of small amount of sulfur [22] seems to be effective in preventing coke formation.

On noble metals (Rh, Ru, Pt and Ir), coke is thought to block the metal and to induce deactivation because of loss of surface metal atoms. There are a lot of debates and controversies among authors about which of these metals presents the best performances [15,23–25]. Rostrub-Nielsen and Hansen compared the catalysts based on Ru, Rh, Pt, Ir, Pd and Ni, and found that Ru and Rh provided high selectivities with carbon free operations and high activities [23]. For supported Rh catalysts, Wang and Ruckenstein concluded that deactivation is strongly dependent on the nature of the support. Among the irreducible metal oxides, γ-Al_2O_3, La_2O_3 and MgO provided stable catalytic activities during 50 h. Deactivation, however, occurred over the SiO_2 and Y_2O_3 supported catalysts [24].

Although Rh seems to be the one that better fulfills with the compromise between activity and stability, platinum is an attractive metal to be used as a catalyst for syngas production due to good availability and its relatively low price with respect to Rh. For Pt/Al_2O_3 catalysts, Nagaoka et al. reported that Pt particles are gradually covered by a coke monolayer, which is correlated to an initial deactivation in DRM [25]. van Keulen et al. [26] showed that Pt is one of the most active and stable metals among zirconia supported group VIII metals and Pt/ZrO_2 has a very high feedstock of $CH_4/CO_2 = 2$. Pompeo et al. [27] reported that Pt/ZrO_2, Pt/α-Al_2O_3–ZrO_2 clearly showed lower deactivation level than Ni/ZrO_2 and Pt or Ni catalysts supported on α-Al_2O_3. Although the γ-Al_2O_3 is one of the most used supports in references, it is thermally unstable at high temperatures (>600 °C) since γ-Al_2O_3 suffers a transformation process into the more thermally stable α-Al_2O_3.

The catalytic group [28,29] found that alkali-leached Ni_3Al powders showed a high catalytic activity for the methanol decomposition. Ma et al. [30] applied atomized Ni_3Al powder for methane steam reforming and they revealed that fine Ni particles, which were produced on the outer surface of Ni_3Al powder during the pretreatment and served as a catalyst, survived on the surface after tests at all the temperatures. They remained almost unchanged below 700 °C, leading to the good stability, while sintering and oxidation occurred at high temperatures, leading to the rapid deactivation.

Thus, taking into consideration many arguments (catalytic performance, availability, cost, industrial application, etc. [4,5,27–33]), it is still important to develop Ni-based catalysts resistant to carbon deposition.

In the present contribution, we consider the advantages of Ni_3Al intermetallide known as a promising high temperature material because of its excellent high temperature strength and good corrosion/oxidation resistance, mechanical tics, and thermal conductivity [34,35].

In our work we pay attention to a novel synthetic approach based on the self-propagating high-temperature synthesis (SHS) [34], combined with the ion implantation (as a method of the surface modification) [36]. SHS is based on rapid, highly exothermic solid flame reactions between powders to produce very high temperatures and stable products containing a high concentration of structural defects, which can act as the active sites in heterogeneous catalysis. This combined method of catalyst preparation was applied successfully to obtain Ni_3Al, containing Ni phase [37–40] and very small Pt particles (from several atoms and more). We found that Ni_3Al exhibits high catalytic activity in DRM but it undergoes partial deactivation at high temperature because of the carbon deposition [41]. Therefore, the subject of the present work is to develop new effective Ni-containing catalyst on the base of Ni_3Al intermetallide and modified with a small amount of noble metal (Pt) that can result in a relatively cheap bimetallic (from the catalytic standpoint) catalyst assuring both, the high activity to syngas production and low carbon deposition.

2. Experimental

2.1. Catalyst preparation

Ni_3Al intermetallide was prepared by the method of SHS [34] using mixture of Ni (Nornickel) and Al (SUAL-PM, Shelekhov) powders preliminarily dried in vacuum at 100 °C for 3 h. The first step of catalyst preparation was performed in the same way as we previously reported [41]. The cost-effectiveness of SHS is associated with (1) utilization of reaction heat instead of electric power (ΔH_f^0 (Ni_3Al) = −157 kJ mol^{-1}), (2) high combustion temperature and burning velocity, (3) simplicity of facilities, and (4) high quality of products. The main parameters of SHS were the following: burning velocity (1 cm s^{-1}), combustion temperatures (1400 °C), induction time for ignition (0.4 s), ignition temperature (900 °C). The powders were not specifically treated in reductive atmosphere because we used powders obtained by electroplating technique, and it was necessary to avoid metal hydrates formation at high SHS temperatures [41]. To achieve optimal density in the SHS process, cylindrically shaped samples were prepared by double-action pressing. The porosity calculated in the current work was about 37%, which is optimal for a basic Ni_3Al component. SHS of pressed samples was performed in volatilizer under constant pressure in argon atmosphere. Heat impulse was supplied to a butt part of the pressed intermediates. For catalytic studies, fractions with particle size of 400–600 μm were selected.

The second step of catalyst preparation was ion implantation by Pt performed in Mevva-V.RU (Metal Vapour Vacuum Arc) setup (designed in Lawrence Berkeley National Laboratory (USA) and improved by the group [42]. A detailed description of the Mevva–V ion source can be found in [43]. In brief, an initiating discharge voltage pulse with an amplitude of 2 kV was produced between the Pt cathode located on the source axis and trigger electrode that led to the ignition of a surface discharge. A vacuum arc was thus ignited between the Pt cathode and the hollow anode. A power supply based on an artificial forming line maintained a vacuum arc discharge current of up to several hundreds of amperes at pulse duration of hundreds of microseconds. The total ion current extracted from the source reached 0.5 A at an accelerating voltage of up to 50 kV. The area of the ion beam cross-section at the output of the extracting system therewith amounted to 100 cm^2. Ni_3Al grains were placed to the holder in front of ion beam with ion current density of 2.3 mA cm^{-2}, average ion energy of 60 keV, frequency 2 Hz in vacuum of 3×10^{-6} Torr. Three Pt-implanted Ni_3Al catalysts with different Pt dosages (1×10^{16}, 5×10^{16} and 1×10^{17} ion cm^{-2}) were prepared. Some catalyst characteristics are presented in Table 1.

2.2. Catalyst testing

Methane reforming with carbon dioxide was carried out in a temperature-programmable quartz tube reactor with inner diameter of 6 mm and a length of 130 mm at temperature range of 600–900 °C, molar ratio CO_2:CH_4 = 1:1 and at ambient pressure. The tube was placed in a vertical tube furnace. The temperature in the catalyst bed was measured by a thermocouple placed inside a quartz thermocouple well with outer diameter of 3 mm. Undiluted catalyst (0.5 cm^3 bulk volume) was used for testing. It is undesirable to use hydrogen for the pretreatment because of the Ni_3Al structural transformation that leads to decrease CH_4 and CO_2 conversions. Besides, during H_2 pretreatment partially oxidized nickel is able to be reduced to metallic Ni and undergo

Table 1
Phase composition and lattice parameters of initial catalysts. BET surface area and Ni_3Al dispersion before/after DRM (reaction conditions: CH_4:CO_2:He = 20:20:60 vol.%, P = 1 atm, V(catalyst) = 1 cm^3, V(CH_4 + CO_2) = 100 cm^3 min^{-1}).

Catalyst	Preparation method	Pt dosage, (ion cm^{-2})	Initial phase composition (in accordance with XRD)	Lattice parameter (nm)	BET surface area (m^2 g^{-1})	Particle diameter for Ni_3Al (nm)
Ni_3Al	SHS	0	Ni_3Al	0.3569	1.1/0.8	28/92
Pt/Ni_3Al-1	SHS + II	1×10^{16}	Ni_3Al	0.3569	1.1/0.9	27/67
Pt/Ni_3Al-2	SHS + II	5×10^{16}	Ni_3Al + (Ni,Al) traces	0.3571	1.2/0.9	25/48
Pt/Ni_3Al-3	SHS + II	1×10^{17}	Ni_3Al + (Ni,Al) + Ni traces	0.3573	1.3/1.1	21/36

anticipatory sintering. Prior to testing the catalyst was heated to 500 °C in helium (50 cm^3/min). After 1 h at this temperature, the feed was switched to reaction gases (CH_4:CO_2:He = 20:20:60 vol%, 100 cm^3 min^{-1}). Then reactor was heated to required temperature (for example, 600, 700, 800 or 900 °C) with 10 °C min^{-1} rate. When the temperature approached the value, the sampling of post-reactor gas phase was started. Analysis of reaction products was carried out by gas chromatography (GC) using Carbosieve SII and Porapak Q packed columns and TCD. After required time on stream (8, 24 or 120 h) at various temperatures, the stream of methane and carbon dioxide was stopped, and the reactor was cooled to room temperature under flow of He. The conversion was calculated on the basis of the feed flow rates and the dry exit gas composition obtained by GC.

2.3. Catalyst characterization

Crystalline portions of Ni_3Al and Pt/Ni_3Al catalysts before and after DRM were identified at room temperature using powder X-ray diffraction using diffractometer Shimadzu XRD-6000 (Cu Ka radiation, λ = 0.154187 nm). Database: PCPDFWIN and POWDER CELL. *In situ* XRD experiments were carried out in the VEPP-3 station of Siberian Synchrotron and Terahertz Radiation Center of Budker Institute of Nuclear Physics of SB RAS. To compare the phase structures of the samples, the count of intensity of diffraction peaks was normalized (λ = 0.1731 nm). Morphology of catalysts was investigated using scanning electron high-vacuum microscope (SEM) VEGAII LMU (Czech Republic) coupled with an X-ray energy dispersive spectroscopy (EDS) system (Oxford INCA Energy 350) and SE (secondary electron) and BSE (backscattering electron) detectors. The surface areas (BET) were determined by nitrogen adsorption using an automated gas adsorption analyzer (ChemiSorb 2750, Micromeritics, USA) linked with mass-spectrometer QMS-300 (Stanford Research System, USA). Thermogravimetry-differential thermal analysis (DTA-TG) measurements were conducted under oxidative (20 cm^3 min^{-1}) atmosphere with STA 409 Luxx (NETZSCH, Germany) using 30–50 mg of samples and with 10 °C min^{-1} increase rate from room temperature to 1000 °C. Transmission electron microscopy (TEM) was performed with JEOL JEM-2010 machine equipped with Gatan slow-scan camera for high-resolution observation and energy-dispersive X-ray microanalyzer (EDX) for elemental analysis of specimen surface. The accelerating voltage applied was 200 kV. The X-ray photoelectron spectroscopy (XPS) patterns were acquired with a Physical Electronic 5700 spectrometer equipped with a hemispherical electron analyser and MgKα X-ray exciting source (1253.6 eV, 15 kV, 300 W). It has been used as an internal patron for calibration C1s (284.4 eV) considering a deviation ±0.2 eV.

3. Results and discussion

In accordance with the phase diagram, the Ni–Al system is characterized by the possible formation of a number of chemical compounds, particularly $NiAl_3$, NiAl, Ni_2Al_3, and Ni_3Al [44]. As we previously reported [37,41], among all these substances, only the Ni_3Al-based system containing small amount of metallic nickel phase revealed maximum catalytic activity during DRM (even at high temperatures of 900–950 °C). Nevertheless, this system underwent the partial deactivation because of coking [41]. Therefore, taking into consideration Pt ability to activate the strong C–H bond (E_{C-H} = 470 kJ mol^{-1})[45], and also low carbon solubility in Pt (0.8 at.% at 876 °C) [44], we decided to input such a desirable noble metal to the Ni_3Al matrix, and use specific method of catalyst treatment like an ion implantation to provide the homogeneous Pt distribution. Three doses were used for implantation: 1×10^{16}, 5×10^{16} and 1×10^{17} ion cm^{-2}. For convenience and simplicity, the catalysts are referred to as Pt/Ni_3Al-1, Pt/Ni_3Al-2, Pt/Ni_3Al-3, respectively (Table 1).

3.1. Catalytic performance

Catalytic activity results have shown that in the case of Ni_3Al intermetallic samples the presence of Pt strongly enhances the catalytic performance (Fig. 1a, b), with an effect which increases with the rise of the Pt content.

The catalyst with the highest Pt content, i.e. Pt/Ni_3Al-3 (1×10^{17} ion cm^2) exhibits highest catalytic activity, for example, CH_4 conversions was 96% at 850 °C, while Ni_3Al catalyst showed only 72%. With respect to the selectivity, expressed as a molar ratio H_2/CO, for all catalysts it is maintained in values between 0.85 and 1 (at 630–650 °C) near to the corresponding stoichiometric relationship for DRM, but the ratio decreases with temperature increase up to 900 °C (Fig. 1c). The lower than 1 value is due to the reverse water gas shift reaction (RWGS) [46]. Moreover, this the ratio decreases with the decrease of Pt content, i.e. Pt provokes H_2 production. There are two reaction steps are responsible for H_2 production [5], i.e. dissociative CH_4 adsorption to form CH_x species and the subsequent surface reaction of CH_x. So, the most likely, Pt is able to activate methane molecule.

Moreover, unmodified Ni_3Al catalyst requires 5–6 h to reach the steady state of working that deals with phase transformations.

Some authors assert that supported Pt catalysts (without Ni) did not show any activity in DRM at all [45], but even small amount (less than 1 wt%) enhances the catalytic performance considerably. Thus, the synergistic catalytic effect of Pt–Ni systems is possible. In this work, the preparation method is extremely important to be discussed. During the process of implantation each individual Pt^{2+} (or Pt^{4+}) ion produces many point defects in the target Ni_3Al crystal on impact such as vacancies and interstitials. In this case the ion collides with a target atom, resulting in transfer of a significant amount of energy to the target atom so that it leaves its crystal site. This target atom then itself becomes a projectile in the solid, and can cause successive collision events. Interstitials result when such atoms (or the original ion itself) come to rest in the solid, but find no vacant space in the lattice to reside. These point defects can migrate and cluster with each other, resulting in dislocation loops and other defects. Moreover, during the implantation the ions with high energy are able to form new unsteady phases (such as Pt–Ni alloys) after the penetration to the crystal lattice of Ni_3Al. So, Pt-implanted catalyst surface is absolutely not the same as the initial Ni_3Al sample.

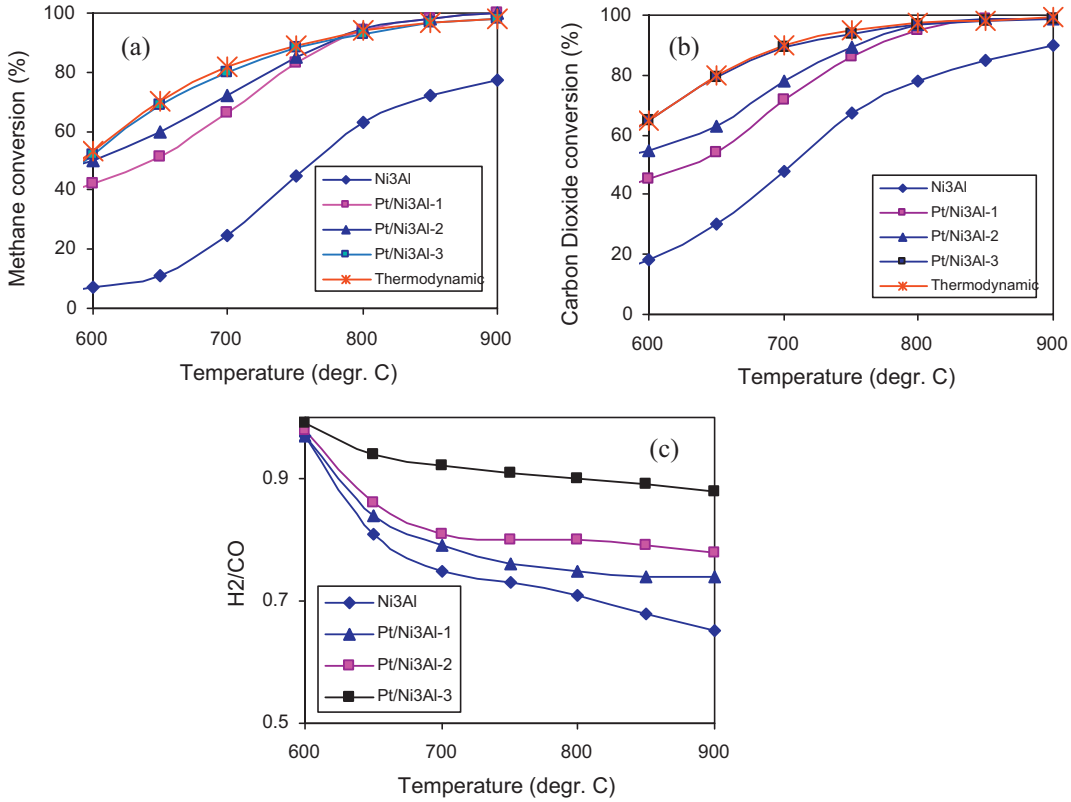

Fig. 1. CH_4 and CO_2 catalytic conversions (a, b) and H_2/CO (c) ratio over Ni_3Al, Pt/Ni_3Al-1, Pt/Ni_3Al-2, Pt/Ni_3Al-3 at 600–900 °C. Reaction conditions: CH_4:CO_2:He = 20:20:60 vol.%, P = 1 atm, V(catalyst) = 0.5 cm^3, V(CH_4 + CO_2) = 100 cm^3 min^{-1}.

It is noticeable that the addition of Pt to the Ni_3Al catalyst remarkably stabilized the catalytic performance and retarded the catalyst deactivation (Fig. 2). The Pt/Ni_3Al-3 catalyst showed methane conversion more than ca.95%, without significant catalyst deactivation even after 120 h catalytic reaction. On the other hand, the Ni_3Al matrix experienced slow deactivation, because reactor plugging occurred due to the coke after 60 h reaction. So, the primary effect of promoter addition is to retard catalyst deactivation by suppressing carbon deposition on the catalyst surface.

Thus, Pt-implanted catalysts have two advantages in comparison with unmodified Ni_3Al: (1) they work without the apparent activation stage and (2) they are stable during 120 h without obvious deactivation.

3.2. Bulk properties of the catalysts

Taking into consideration the low portions of Pt in the samples and some difficulties in Pt detection by usual methods, the catalyst with the highest catalytic activity and Pt content (Pt/Ni_3Al-3) was selected for comparison with Ni_3Al matrix. X-ray diffraction patterns of Ni_3Al and Pt/Ni_3Al-3 before and after the catalytic reaction are shown in Fig. 3. It can be seen, the phase assigned to well-crystallized Ni_3Al structure was detectable in initial samples, and no Pt diffraction peaks were observed for modified catalyst (even with the highest Pt dose), that means well dispersed Pt on the surface of Pt/Ni_3Al-3 catalysts. After DRM, the disordering transformations happens in both catalysts for the occurrence of (Ni,Al) solid solution (the solution of Al in Ni) and Ni phase.

The bulk lattice constant for Ni_3Al phase in initial unmodified sample, a = 0.35699 (±0.00005) nm was calculated from these XRD spectra (taken at room temperature). In Pt/Ni_3Al-3 this value was 0.35701 nm that means the presence of defects of crystal lattice induced by ion implantation. After the catalytic tests at 800° for

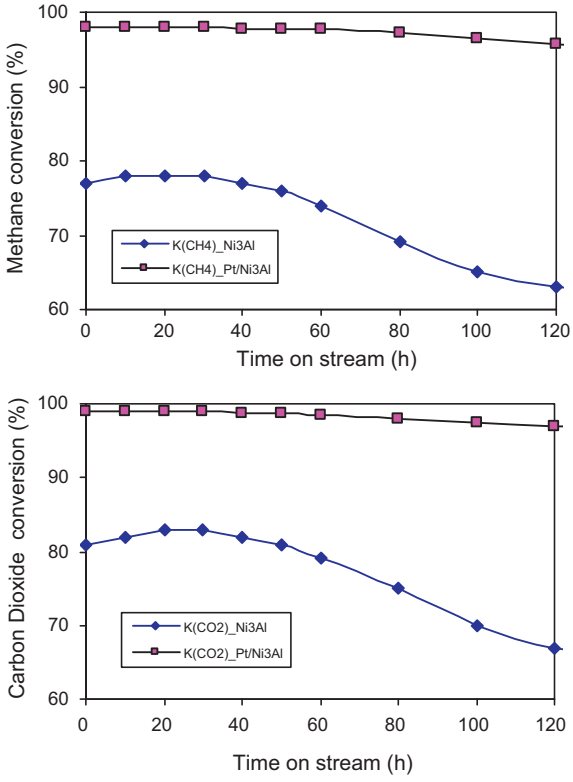

Fig. 2. Stability test for Ni_3Al and Pt/Ni_3Al-3 catalysts during DRM. (Reaction conditions: 900 °C, V(CO_2:CH_4:He = 20:20:60 vol.%) = 100 cm^3 min^{-1}.)

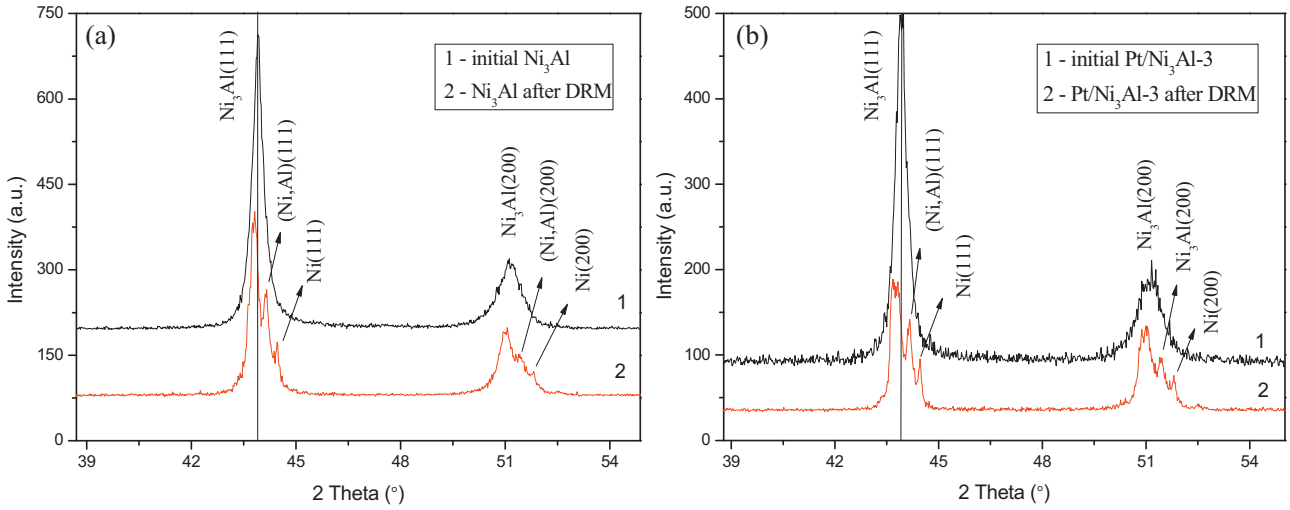

Fig. 3. XRD patterns of Ni_3Al and Pt/Ni_3Al-3 catalysts (a) before and (b) after DRM. (Reaction conditions: 900 °C, time on stream 24 h, CO_2:CH_4 = 1:1.)

24 h the Ni_3Al lattice parameter becomes equal to 0.35796 nm for unmodified catalyst, and 0.35807 nm for Pt/Ni_3Al-3. So, lattice parameters have increased after DRM. The most reasonable explanation for this phenomenon is carbon (formed after the CH_4 dissociation) diffusion inside the Ni_3Al crystal lattice [5]. But some relaxation effects after the high temperature treatment may induce the same changes, therefore, to understand the catalyst behaviour during DRM and to differentiate the temperature and reaction effects, the structure of Ni_3Al superlattice and its transformations were studied by high-resolution X-ray diffraction method using a synchrotron radiation.

3.3. Evolution of microstructure

In situ XRD spectra of Ni_3Al and Pt/Ni_3Al-3 are shown in Figs. 4 and 5. The superlattice diffraction peaks of (1 0 0) and (1 1 0) crystal planes of Ni_3Al phase are present in both cases, that means the existence of long-rang order in the intermetallide crystal lattice.

No obvious changes are observed in the XRD patterns during the reaction till 550 °C. After the heating above 600 °C, the (Ni,Al) solid solution and Ni diffraction peaks appear, which means Ni_3Al is reordering under the temperature effect and DRM environment. With temperature increasing, the metallic Ni phase becomes clearly detectable, implying that the fine Ni particles agglomerate. It can also be seen from Figs. 4 and 5 that the diffraction peaks sharpen for both samples. The changes of diffraction peak shape mean the changes of grain size and microstrain. It should be pointed that the nanocrystallites heated at 750 °C and above grow to more than 100 nm that is not suitable to calculate grain size and microstrain from XRD data. So, the system on the base of Ni_3Al reconstructs partially, supplying Ni phase additionally (and (Ni,Al) solid solution as well) and defects annealing also takes place.

The most important information can be derived from the comparison of the strongest diffraction peaks of (1 1 1) crystal planes (Fig. 4b and 5b). First of all, the intensity and diffraction peaks shape are different, for example, the peak of Ni_3Al is symmetric and more intense than that for Pt/Ni_3Al-3, therefore, the first sample has a higher degree of crystallinity, while the second one is more amorphous and contains very small quantities of (Ni,Al) solid solution and Ni phases. These effects are the result of non-equilibrium character of catalysts synthesis and further modification, the structure of the initial samples become defect saturated and show strong broadening of X-ray diffraction lines, especially after implantation.

With heating disordering transformations approximately the same in both samples and after the heating above 750 °C, the diffraction peak of $Ni_{0.9}Al_{1.1}$ (1 1 0) appears, that means the microstructure evolution is proceeding at high temperatures in both samples. In addition, the remarkable diffraction peak shifts to the low-angle region are observed for Ni_3Al phase in both catalysts, that means the lattice parameter increases with temperature. Thus, this is mostly a temperature factor.

In order to exclude the temperature impact, DRM was performed in the reactor chamber at constant temperature of 800 °C for 1 h after the heating in He atmosphere. Nevertheless, the noticeable diffraction peak shift was observed as well. One can see the shift of intermetallide reflections to the small angle side indicating the increase of lattice constant for 0.0015–0.002 nm while the lattice constants of (Ni,Al) solid solution and metallic Ni remain the same (Fig. 6). Furthermore the intensity of intermetallide reflections becomes smaller whereas Ni reflections increase. This is mainly a reaction impact.

Here, we can summarize the following: (1) the lattice parameter changes of corresponding phases in Ni_3Al and Pt/Ni_3Al-3 have the same trends, (2) Ni_3Al lattice parameter of unmodified catalyst increases faster than that of the modified sample, especially for the first 25 min on $CH_4 + CO_2$ stream.

It has been suggested [47] that carbon atoms, formed by methane decomposition on the (1 0 0) and (1 1 0) nickel surface, diffuse across the Ni particles and deposit on the (1 1 1) surface, forming ordered graphite layers aligned parallel to the metal–carbon interface. In our case the Ni_3Al phase has the similar type of crystal lattice as Ni phase but with a slightly larger parameter constant, therefore, C penetrates into the lattice of intermetallide easier than in nickel one, inducing lattice constant increase. In the Ni_3Al sample no special hindrances for carbon diffusion. In the case of the Pt/Ni_3Al-3 sample, well-dispersed Pt (which has a low carbon solubility and does not form the stable carbides), being in the intimate contact with Ni, physically and energetically impedes the diffusion of carbon atoms into the Ni_3Al crystal lattice.

3.4. Surface characterization

3.4.1. BET surface area

The BET surface areas of the intermetallides before DRM reaction are listed in Table 1. Initial surface areas were (quite small, for example, 1.1 $m^2\,g^{-1}$ for Ni_3Al and 1.3 $m^2\,g^{-1}$ Pt/Ni_3Al-3. The

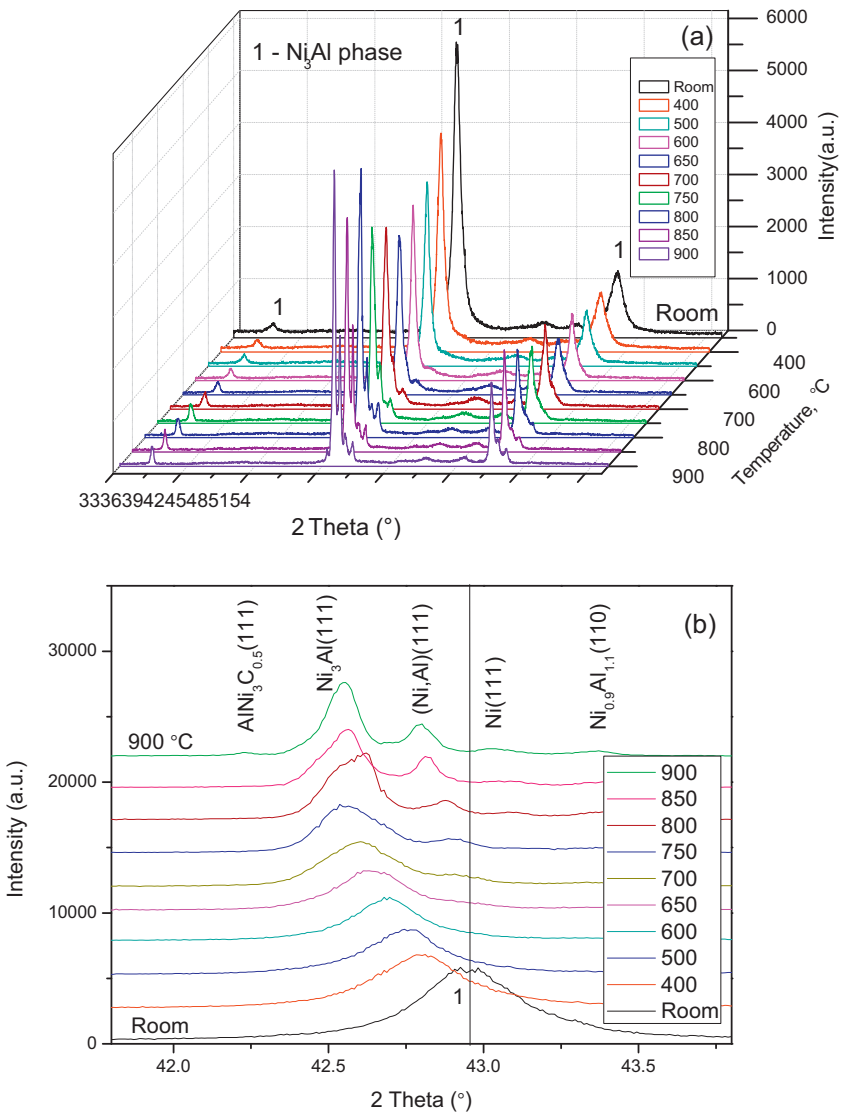

Fig. 4. *In situ* XRD patterns of Ni_3Al catalyst during DRM at temperatures from 400 to 900 °C: (a) general view, (b) fragment (2θ = 42–44°) for precise observation. The first pattern (at room temperature) is given for comparison.

surface areas decreased slightly after reaction at 600 °C. At higher temperature above 800 °C, the surface area decreased significantly to approximately one quarter. In principle, it is expected that the Ni particles gradually aggregate and sinter on the surface of the catalyst. XRD investigations confirmed the partial destruction of Ni_3Al phase with Ni phase release, but nickel nanoparticles formed after this lattice reconstruction have high level of free Gibbs energy, therefore, according to the general tendency to minimize free energy, they will undergo coalescence, especially at high DRM temperatures.

3.4.2. XPS

The XP spectra of Ni2p of initial and used Ni_3Al catalysts are presented in Fig. 7. The different states could be distinguished by standard fitting procedure. For the initial Ni_3Al sample Ni2p can be deconvoluted in three components centered at 852.04, 855.35 and 856.05 eV. These signals can be associated with Ni^0, Ni(II), probably as NiO or $NiAl_2O_4$ due to the asymmetry of the signal, and the third component can be assigned with Ni(II) as well. The other signals are the satellites and doublets. The Al2p spectrum showed three chemical states for Al; the signal centered at 71.37 eV associated with the binding energy (BE) to metallic state of Al (Ni_3Al), the second signal localized at 73.96 eV corresponding to Al-oxide (AlO_x or Al_2O_3) as amorphous component, the third signal localized at 76.15 eV for possible formation of $NiAl_2O_4$.

After the catalytic tests Ni2p can be deconvoluted in three components again, centered at 852.54, 855.80 and 857.05 eV. These signals can be associated with Ni^0, Ni(II) probably as NiO or $NiAl_2O_4$ due to the asymmetry of the signal and the third component can be assigned to Ni(II). The Al2s spectrum showed four chemical states of Al; the signal centered at 110.85, 114.25, 118.74 and 120.53 eV. The first signal could be associated tentatively with the shift of BE associated with Ni_3Al, the second signal localized at 114.25 eV corresponding to Al-oxide (AlO_x), the third one at 118.74 eV corresponds to Al_2O_3 as amorphous component and the last component relates to the formation of $NiAl_2O_4$. Thus, we can conclude that Ni^0 oxidized into NiO and $NiAl_2O_4$ (partially, on the surface only) during DRM and Al^0 oxidized into Al_2O_3 (different modifications) and spinel as well. It leads to decrease of catalytic activity and stability in aggressive atmosphere of DRM.

The XP spectra of Ni2p of initial and used Pt/Ni_3Al-3 catalysts are presented in Fig. 8.

In general, they are similar to the spectra of unmodified catalyst but we can observe the BE shift (the main signals: 852.56, 854.18

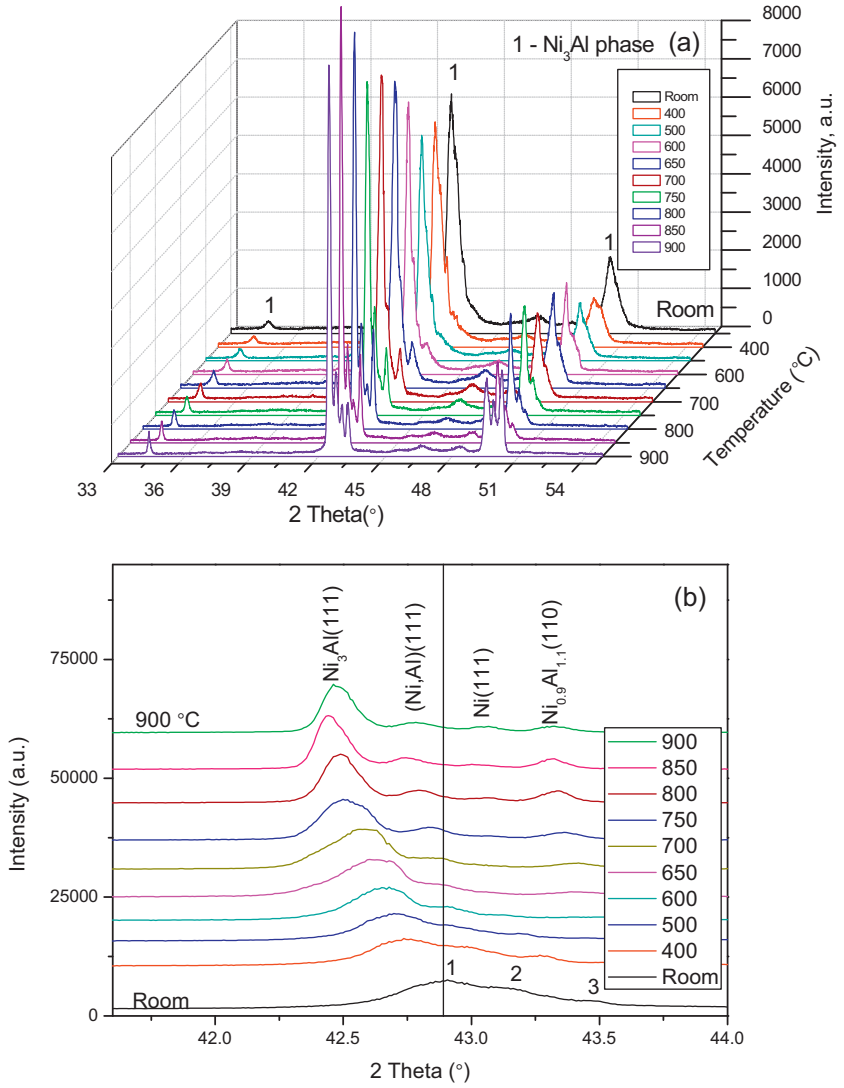

Fig. 5. *In situ* XRD patterns of Pt/Ni_3Al catalyst during DRM at temperatures from 400 to 900 °C: (a) general view, (b) fragment (2θ = 42–44°) for precise observation ((1) Ni_3Al, (2) (Ni,Al) solid solution, (3) Ni phases). The first pattern (at room temperature) is given for comparison.

and 856.10 eV) and relative content of different states are different. For example, Ni^0:Ni^{2+} ratios (%) are the following: 8.62:91.38 (initial Ni_3Al); 7.21:92.79 (used Ni_3Al); 9.72:90.28 (initial Pt/Ni_3Al-3); 10.99:89.01 (used Pt/Ni_3Al-3). So, nickel state evolution during DRM in these two catalysts has the opposite trends, i.e. Ni^0 percentage decreases (8.62 → 7.21) in Ni_3Al, and it increases (9.72 → 10.99) in Pt/Ni_3Al catalyst.

XPS Pt4d pattern over used Pt/Ni_3Al-3 is shown in Fig. 9. It is seen that only one species with a BE of 314.4 eV (corresponds to Pt^0) is generally formed on the catalyst surface. It is notable, that before reaction also one peak was registered in the Pt4d spectrum (BE = 314.8 eV). So, Pt is stable in severe reductive–oxidative conditions of DRM.

Thus, addition of Pt in Ni_3Al catalyst leads to a better reducibility of nickel oxide particles, a better dispersion of the intermetallide (Table 1) and nickel particles, and as a consequence, high activity and stability of Pt/Ni_3Al catalysts in the reaction of CO_4–CO_2 reforming.

3.4.3. BSE microscopy observation

3.4.3.1. Ni and Al distribution. SEM observation was performed on the initially pressed Ni and Al powders and half-finished Ni–Al product prepared by SHS, using BSE mode (Fig. 10) and EDS analysis.

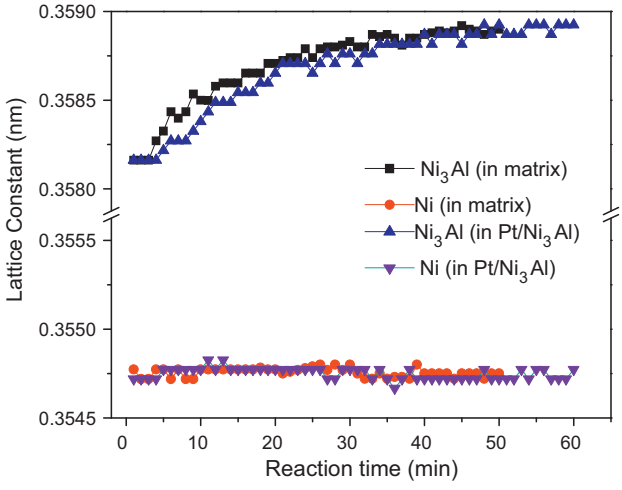

Fig. 6. Lattice parameter changes of Ni_3Al and Ni phases with time during CH_4–CO_2 reforming at 800 °C, V(CO_2:CH_4:He = 20:20:60 vol.%) = 50 cm^3 min^{-1}, Anton Paar's XRK 900 Reactor Chamber).

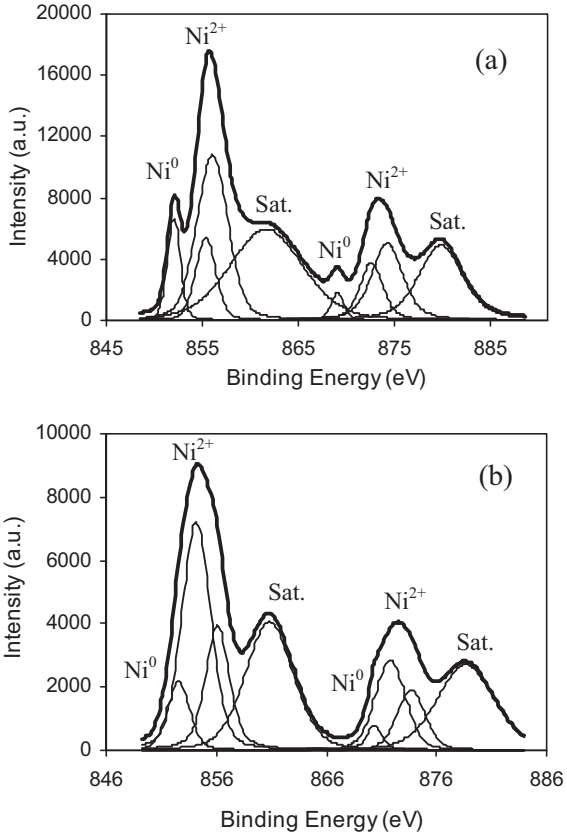

Fig. 7. XP spectra of Ni 2p of Ni_3Al (a) before and (b) after DRM (900 °C, 24 h).

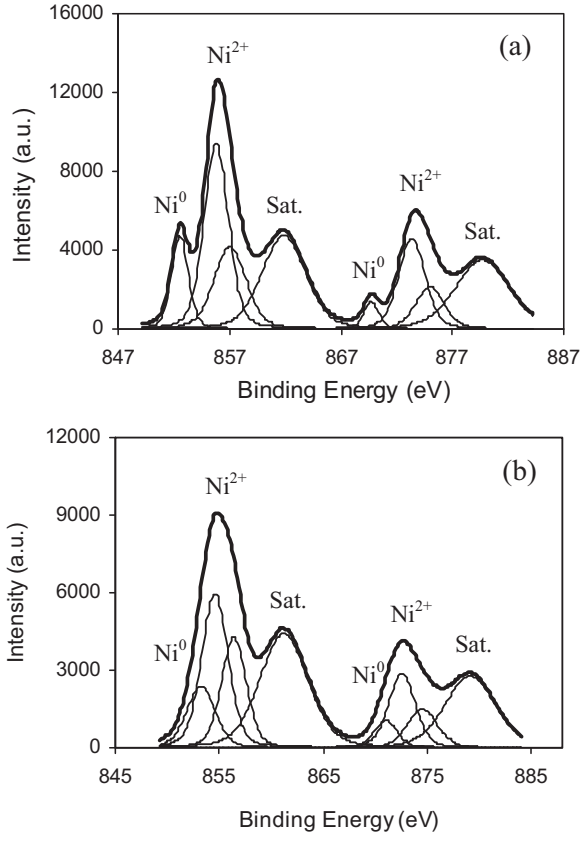

Fig. 8. XP spectra of Ni 2p of Pt/Ni_3Al-3 (a) before and (b) after DRM (800 °C, 24 h).

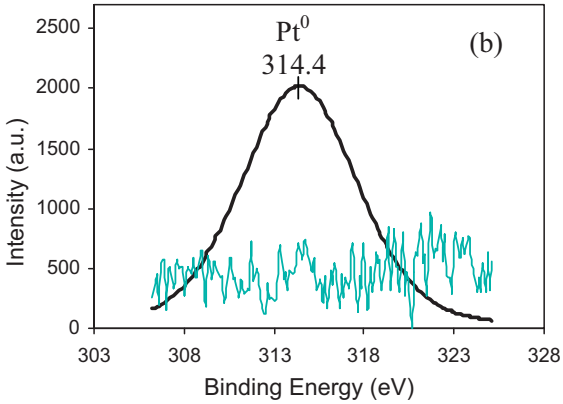

Fig. 9. XPS profile of Pt 4d for Pt/Ni_3Al-3 catalyst after DRM (800 °C, 24 h).

In micrograph the contrast is generated by the atomic number therefore two different contrasts are observed which suggests two different phases. The light gray (almost white) regions correspond to the Ni phase while the dark regions correspond to the Al phase. Fig. 10a shows that the distribution of initial powders is uniform enough but the size of the particles can reach 20–30 μm.

Fig. 10b is an image which corresponds to the specimen with 13.4 wt% of Al and 86.4% Ni, prepared by SHS (without modification). According to the contrasts there are several phases there: dark matrix, bright spots and the thin gray layer, which is located

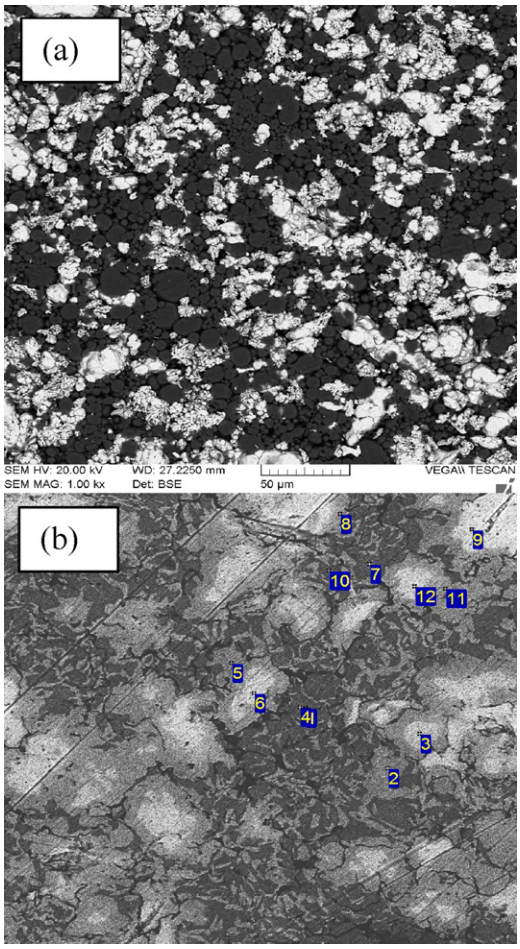

Fig. 10. Backscattered electron images of the (a) pressed Ni and Al powders before SHS and (b) half-finished Ni–Al product prepared by self-propagation high temperature synthesis.

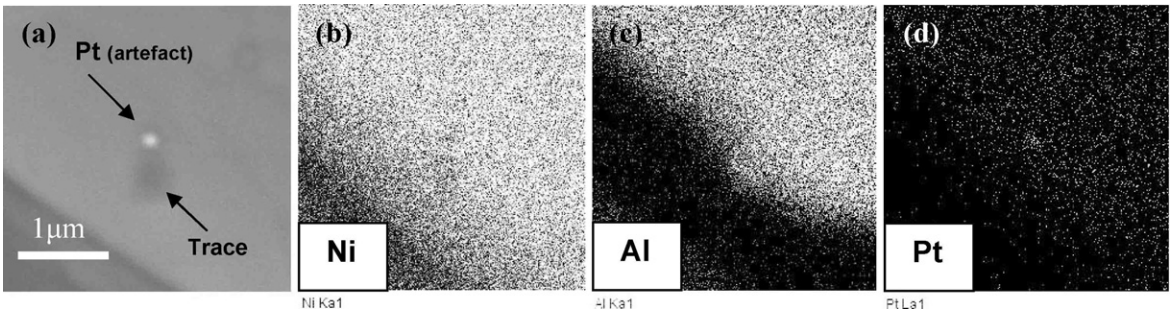

Fig. 11. Backscattered electron images of the (Pt/Ni_3Al-3) surface (distribution of Ni, Al and Pt after ion implantation).

between dark and bright regions. EDS analysis (Table 2) was performed on several points (Fig. 10b, points 3, 6, 9, 12) and revealed that these regions are highly concentrated in Ni (with respect to the stoichiometric Ni_3Al phase). On the other hand, the dark regions are enriched in Al (Fig. 10b, points 1, 4, 7, 10). At last, the thin layer corresponds to Ni_3Al phase (Fig. 10, points 2, 5, 8, 11). So, after the application of the SHS method of catalyst preparation, the elements are distributed inhomogeneously across the catalyst grain.

3.4.3.2. Pt distribution. Distribution of Pt is very homogeneous (Fig. 11). The majority of Pt particles have the size from several angstroms to several nanometers.

In spite of the camber of the surface, this picture was selected for the observation because it demonstrates not only element distribution on the surface, but also the presence of some droplets. The particle indicated by solid arrows (Fig. 11a) is caused by deposition of liquid droplets of Pt on the Ni_3Al surface during MEVVA ion implantation. Such liquid droplets are known [36] to be ejected from the arc root (also called cathode spots) of the MEVVA ion source. These Pt droplets travel with the plasma and get deposited randomly on the substrate surface. Such Pt is external to the Ni_3Al surface and is not implanted into the Ni_3Al lattice. These liquid droplets are usually called 'macroparticles' (MP) to emphasize their massive size (200–400 nm) compared to the plasma particles produced in the ion source. These macroparticles are the artefacts of the MEVVA ion source. Fig. 10a shows the trace drilled by Pt droplet during MEVVA ion implantation.

In this context, taking into consideration very homogeneous Pt distribution, ion implantation is a promising technique due to its ability to form surface embedded nanoparticles that provide better adhesion. Also, being an integral part of the substrate lattice the Pt nanoclusters formed by ion implantation are free from impurities and their size distributions can be accurately controlled by optimizing ion beam parameters.

Table 2
Elemental composition in different points on the surface of Ni_3Al slice.

Spectrum	Al	Ni
1	21.15	78.85
2	15.06	84.94
3	9.82	90.18
4	21.50	78.50
5	15.38	84.62
6	8.15	91.85
7	20.92	79.08
8	15.03	84.97
9	6.61	93.39
10	21.69	78.31
11	15.08	84.92
12	8.01	91.99

All results (wt%) are normalized.

3.4.4. Morphology and carbon deposition

Fig. 12 shows the SEM micrographs of unmodified Ni_3Al catalysts before and after DRM. The surface is rough before the reaction. The fine nickel particles exist on the surface, though they are not visible by means of SEM. After DRM at 900 °C there are two different types of carbon deposits detected on the surface of Ni_3Al.

The first one is "globular" carbon (Fig. 12b), and the second type is carbon fibers (Fig. 12c). "Globular" carbon covers approximately 20–30% of the surface (it depends on the temperature and time on stream), and it blocks physically the active sites of the catalyst. Among all the Ni particles, only those of them which have large size (more than 50 nm) were mainly covered by such type of

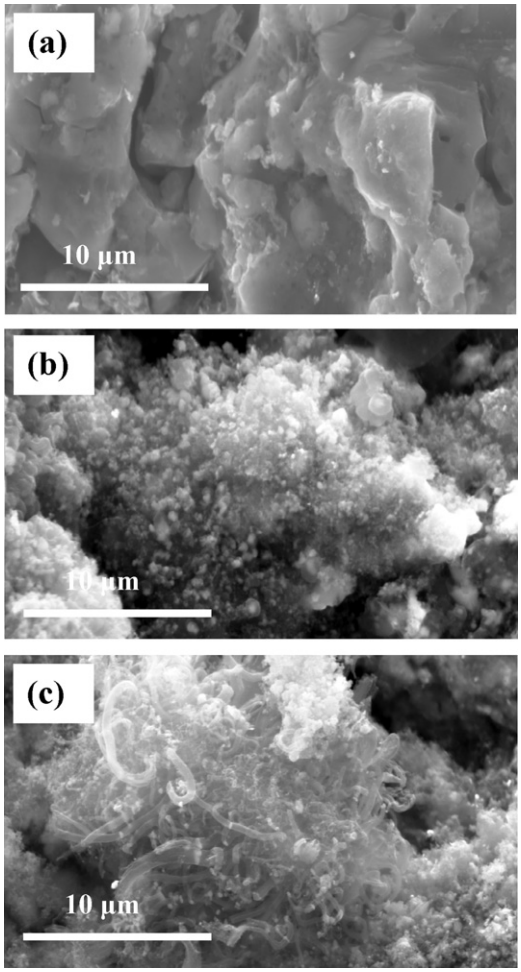

Fig. 12. Morphology of Ni_3Al catalyst: (a) before DRM, (b) "globular" carbon and (c) carbon fibers formed on the surface after DRM for 24 h at 900 °C.

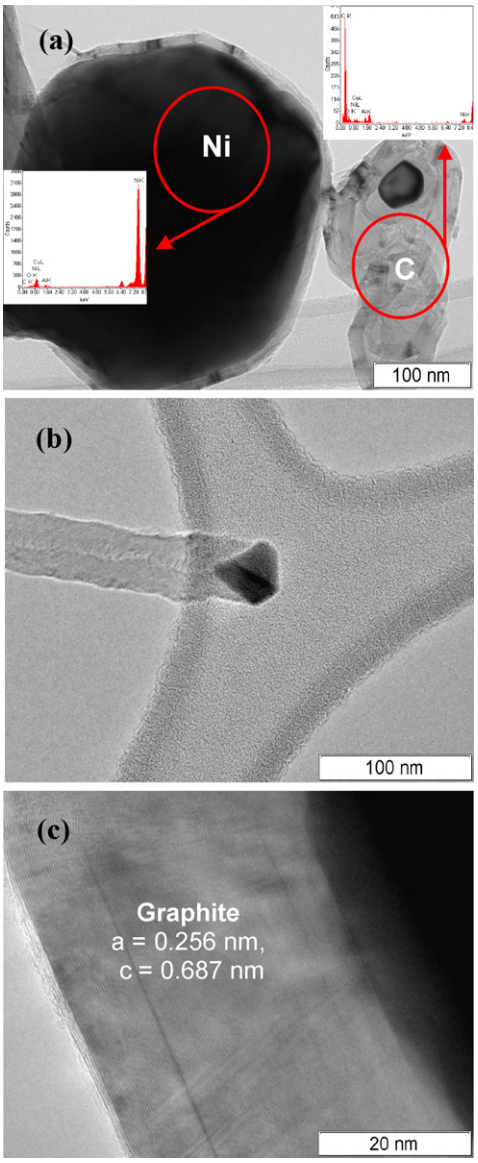

Fig. 13. TEM images of various carbon deposits formed on Ni_3Al surface during DRM for 24 h at 900 °C.

carbon. Perhaps, it depends on the distribution of Ni phase, whish is included in intermetallide structure. Some parts of the surface were covered by the amorphous carbon but, the most likely, it is the precursor of more structured forms (graphene, etc.).

Transmission electron microscopy examination of catalytically grown carbon confirmed the existence of graphene layers (with the thickness of 20–50 nm) and carbon nanofibers produced from the interaction of an Ni_3Al catalyst with methane and carbon dioxide at 900 °C for 24 h (Fig. 13). One carbon fiber grows from one catalytic particle, and the graphite planes in filaments are arranged as coaxially cones (Fig. 13b). The average diameter of carbon filament and the catalyst particle is identical (30–60 nm). Some fragments of the surface were covered by the carbon layers with a graphite structure (Fig. 13c). An increase in the reaction temperature results in the decrease of d_{002} from 0.343 to 0.339 nm (from XRD data) which is close to that of perfect graphite (d_{002} = 0.335 nm).

In principle, it is expected at the formed carbon was deposited on the active sites. According to the reported carbon deposition mechanism [4], the origin of inactive carbon during dry reforming originated from the Boudouard reaction ($2CO \rightarrow C + CO_2$) and from methane decomposition ($CH_4 \rightarrow C + 2H_2$), which are favorable under the conditions of methane reforming with CO_2 (the last reaction especially).

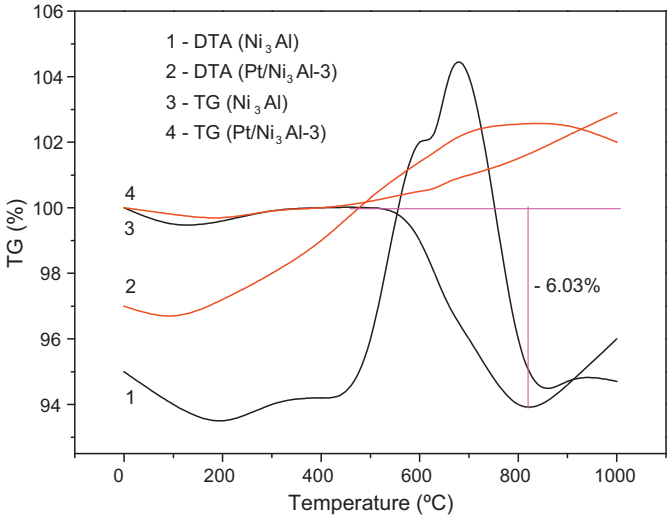

Fig. 14. DTA-TG patterns of Ni_3Al and Pt/Ni_3Al-3 after DRM for 24 h at 900 °C.

The amount of deposited carbon on the surface of the catalysts was evaluated by DTA-TG measurements of the spent Ni_3Al catalysts during DRM for 24 h at 900 °C. These results are presented in Fig. 14.

The slight weight loss occurring at around 100–200 °C was resulted from the evaporation of moisture. However, the carbon deposits over Ni_3Al were oxidized at around 500–800 °C. According to TG analysis 6–12% of coke was formed on the surface of Ni_3Al but this catalyst was active and stable enough during 24 h on stream. Meanwhile, two regions with maxima around 590 and 680 °C were identified, which are in consistent with the literature [48]. Chen at al. [48] have designated these peaks as C_α and C_β. First of them, C_α was the active species responsible for the formation of synthesis gas while C_β the most inactive species, was responsible for catalyst deactivation. So, by means of DTA-TG two types of carbonaceous species formed on these catalysts were detected. But, taking into consideration XPS data, the C1s spectra of spent Ni_3Al catalyst can be deconvoluted in three components localized at 284.8 (dominant peak), 285.65 and 288.71 eV. The signals correspond to graphitic-like carbon, carbonyl groups and carboxyl groups, respectively. The small C=O and C–O contribution, probably, originates from the interaction of CO_2 reagent on the metallic surface. It means that carbon deposits can contain –C–C– and C–O– bonds in their structure, but these groups can be included in one type of deposites.

Therefore, taking into account all methods of investigation, it is reasonable to recognize the existence of two main types of deposits ("globular" carbon consisting of graphene layers, surrounding big particles, and blocking the active sites physically, and as a conse-

Table 3
EDS elemental analysis in several points on the surface of Pt/Ni_3Al-3 catalyst after DRM reaction.

Spectrum	O	Al	Ni	C
1	17.90	22.91	56.47	2.72
2			100.00	0.00
3	15.59	20.91	61.66	1.84
4			100.00	0.00
5	1.07	0.95	97.58	0.40
6	17.58	21.68	57.14	3.60
7	1.63	1.95	96.36	0.06
8	2.64	2.92	93.07	1.37
9	17.50	20.47	58.84	3.19

All results (wt%) are normalized.

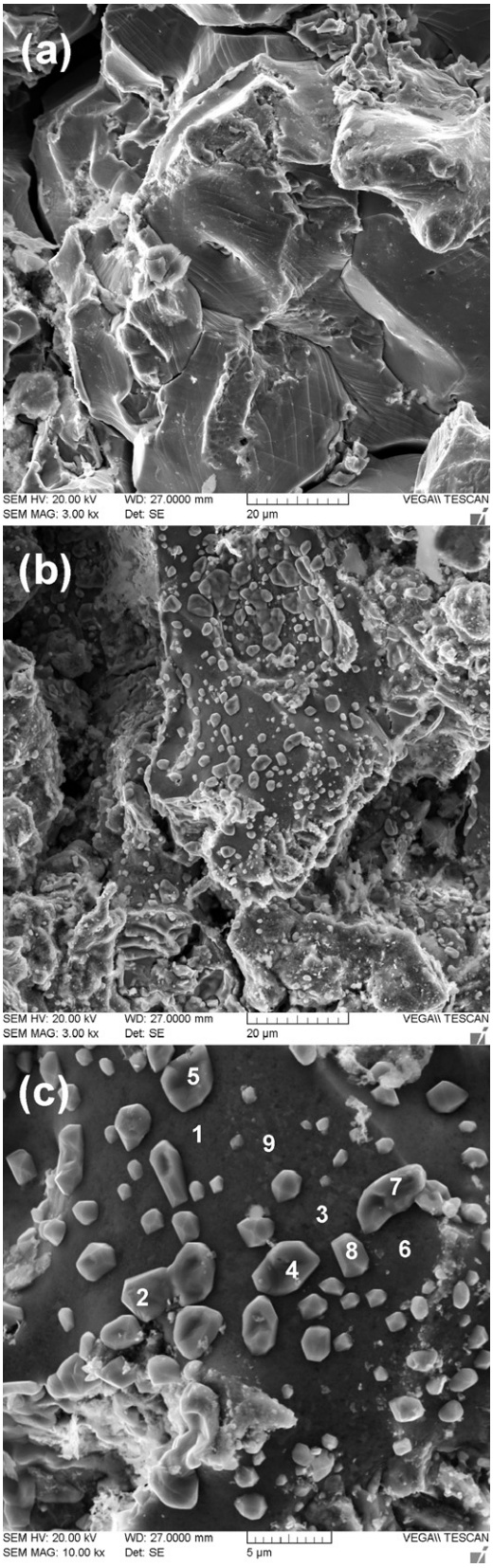

Fig. 15. SEM micrographs of (a) initial Pt/Ni_3Al-3, (b) and (c) Pt/Ni_3Al after DRM during 24 h at 800 °C (CO_2:CH_4 = 1:1, V(CO_2 + CH_4) = 100 cm^3 min^{-1}).

quence, extremely deactivating the catalyst) and the carbon fibers (they induce the catalyst erosion of Ni_3Al, but they do not strongly influence the catalytic activity).

It is clear that the weight loss revealed by TG curves of the used catalysts is due to removal mainly of deposited carbon on the active sites of Ni^0. The contribution from metal oxidation is negligible during temperature-programmed oxidation of both catalysts. Therefore, the TGA-TG results clearly show that a certain amount of coke was deposited on the surface of used catalyst, with an exception of the Pt/Ni_3Al catalyst (Fig. 14, curves 2 and 4). Most probably, the high resistance of this sample against carbon deposition is due to less accessible metallic nickel species.

Indeed, the Pt/Ni_3Al-3 catalyst has the opposite ability to coking. The SEM images of Pt/Ni_3Al-3 surface before and after DRM are shown in Fig. 15 and EDS analysis is given in Table 3.

The surface is typical for alloy cleavage with some flat areas. After the catalytic tests at 600–900 °C this surface was not significantly changed. There are no any regions covered by carbon deposits. Nevertheless, in spite of this favorable effect some parts of the surface were decorated with Ni crystallites (proved by local EDS, Table 3, Points 2, 4, 5, 7, 8).

Therefore, introduction of very small amount of well-dispersed Pt significantly causes an increase in specific activity and a rise in the catalysts resistance to coking. These data are in consistent with the literature [32,45].

The driving force for carbon diffusion and for the global process of carbon filament formation is the difference in solubility at the gas/metal interface and the carbon filament/metal interface. According to the model proposed by Snoeck et al. [49], the nucleation of filamentous carbon is caused by the formation of a solution of carbon in nickel that is supersaturated with respect to filamentous carbon. The degree of supersaturation is determined by the affinity for carbon formation of the gas phase. However, the solubility of carbon in nickel is lowered by the presence of additives (such as Pt) ("dilution" effect) in its lattice and the supersaturation necessary for whisker-like carbon filaments cannot be attained. The improvement of the reforming performance can also be attributed to the formation of two-dimensional surface defects and dislocations as well formed during SHS and ion implantation.

4. Conclusions

(1) This work concentrates on a new type of the catalysts for DRM. Instead of traditional supports on the base of metal oxides, we propose to use material on the base of Ni_3Al superalloy because of its excellent thermal conductivity, high temperature strength, good corrosion/oxidation resistance and mechanical tics. In severe redox DRM atmosphere at high temperature (800–900 °C), Ni_3Al matrix undergoes weak phase transformations, supplying pure Ni nanoparticles, served as the active sites for methane and carbon dioxide activation.

(2) Pt was embedded to the Ni_3Al matrix by means of ion implantation in extremally dispersed state (from several angstroms to several nanometers) in order to stabilize Ni nanoparticles physically and energetically. It means that the presence of a very small (less than 0.1 wt%) amount of extremally dispersed Pt in Ni_3Al catalyst strongly affects the surface and catalytic performance towards the CH_4–CO_2 reforming. Pt implantation leads to easier reduction of nickel oxide species and better dispersion of Ni_3Al particles (as a supplier of active Ni species). Moreover, the ion implantation method induces the dislocation and defect formation.

So, in this work we pay special attention to a novel synthetic approach based on the self-propagating high-temperature

synthesis (SHS), combined with the ion implantation (as a method of the surface modification).

On the base of characterization and catalytic activity data the following conclusions can be drawn as well:

(1) The unmodified Ni_3Al catalyst revealed good activity in DRM at temperatures of 600–900 °C. But this catalyst undergoes partial deactivation because of carbon deposition.
(2) Two types of carbon deposits on the Ni_3Al surface were observed ("globular" carbon consisting of graphene layers, surrounding big (>50 nm) particles, and blocking the active sites physically, and as a consequence, deactivating the catalyst extremely) and the carbon fibers (they induce the catalyst erosion of Ni_3Al, but they do not strongly influence the catalytic activity). The carbon formation on the surface of the catalyst depends on the size of nickel metal particles; the higher coke resistance is observed on smaller Ni particles.
(3) Pt-implanted catalysts have two main advantages in comparison with unmodified Ni_3Al: (a) they work without the apparent activation stage, (b) they are stable during 120 h without obvious deactivation.

In general, this work has demonstrated the novel possibilities of catalyst synthesis by means of SHS and modification of the surface with ion implantation.

Acknowledgements

We gratefully acknowledge Dr. E.M. Oks, Dr. G.Yu. Yushkov, Dr. K.P. Savkin (Institute of High Current Electronics, Siberian Branch of the Russian Academy of Sciences) for the help in ion implantation and Dr. M.R. Sharafutdinov for technical support during *in situ* XRD measurements in VEPP-3 station of Siberian Synchrotron and Terahertz Radiation Center (Budker Institute of Nuclear Physics of SB RAS).

References

[1] B. Steinhauer, M.R. Kasireddy, J. Radnik, A. Martin, Appl. Catal. A 366 (2009) 333.
[2] C. Song, A.M. Gaffney, K. Fujimoto (Eds.), Proc. ACS Symp. Ser. American Chemical Society, Washington, DC, 2002.
[3] (a) M.M. Halmann, M. Steinberg, Greenhouse Gas Carbon Dioxide Mitigation: Science and Technology, Lewis Publishers, Boca Raton, FL, 1999; (b) H. Gunardson, Industrial Gases in Petrochemical Processing, Marcel Dekker, New York, 1998.
[4] M. Bradford, M. Vannice, Catal. Rev. Sci. Eng. 41 (1999) 1.
[5] M.C. Bradford, M.A. Vannice, J. Catal. 173 (1998) 157.
[6] T. Inui, K. Saigo, Y. Fujii, K. Fukioka, Catal. Today 26 (1995) 295.
[7] J.-Y. Ren, W. Qin, F.N. Egolfopoulos, H. Mak, T.T. Tsotsis, Chem. Eng. Sci. 56 (2001) 1541.
[8] P. Ferreira-Aparicio, C. Márquez-Alvarez, I. Rodrıïguez-Ramos, Y. Schuurman, A. Guerrero-Ruiz, C. Mirodatos, J. Catal. 184 (1) (1999) 202.
[9] J. Zhang, H. Wang, A.K. Dalai, J. Catal. 249 (2007) 300.
[10] K. Takeishi, Biofuels 1 (1) (2010) 217.
[11] T.A. Semelsberger, R.L. Borup, H.L. Greene, J. Power Sources 156 (2006) 497.
[12] A.T. Aguayo, J. Erena, I. Sierra, M. Olazar, J. Bilbao, Catal. Today 106 (2005) 265.
[13] A.E. Castro Luna, M.E. Iriarte, Appl. Catal. A 343 (2008) 10.
[14] V.C.N. Kroll, H.M. Swaan, C. Mirodatos, J. Catal. 161 (1996) 409.
[15] W.K. Jozwiak, M. Nowosielska, J. Rynkowski, Appl. Catal. A 280 (2005) 233.
[16] W.D. Zhang, B.S. Liu, Y.L. Tian, Catal. Commun. 8 (2007) 661.
[17] J.T. Richardson, S.A. Paripatyadar, Appl. Catal. 61 (1990) 293.
[18] T. Kodama, T. Shimizu, K.I. Shimizu, T. Kitayama, Energy Fuels 16 (2002) 1016.
[19] B.S. Liu, C.T. Au, Appl. Catal. A 244 (2003) 181.
[20] J.C.B. Wang, S.Z. Hsiao, T.J. Huang, Appl. Catal. A 246 (2) (2003) 197.
[21] N.N. Sazonova, V.A. Sadykov, A.S. Bobin, S.A. Pokrovskaya, E. Gubanova, React. Kinet. Catal. Lett. 98 (1) (2009) 35.
[22] V.R. Choudhary, B.S. Uphade, A.S. Mammam, Appl. Catal. A 168 (1998) 33.
[23] J.R. Rostrub-Nielsen, J.H. Bak-Hansen, J. Catal. 144 (1993) 38.
[24] H.Y. Wang, E. Ruckenstein, Appl. Catal. A 204 (2000) 143.
[25] K. Nagaoka, K. Seshan, K. Aika, J. Lercher, J. Catal. 197 (2001) 34.
[26] A.N.J. van Keulen, M.E.S. Hegarty, J.R.H. Ross, P.F. van den Oosterkamp, Stud. Surf. Sci. Catal. 107 (1997) 537.
[27] F. Pompeo, N.N. Nichio, M.V.V.M. Souza, D.V. Cesar, O.A. Ferretti, M. Schmal, Appl. Catal. A 316 (2007) 175.
[28] Y. Xu, S. Kameoka, K. Kishida, M. Demura, A. Tsai, T. Hirano, Intermetallics 13 (2005) 151.
[29] D.H. Chun, Y. Xu, M. Demura, K. Kishida, D.M. Wee, T. Hirano, J. Catal. 243 (2006) 99.
[30] Y. Ma, Y. Xu, M. Demura, T. Hirano, Appl. Catal. B 80 (2007) 15.
[31] H. Jeong, K.I. Kim, D. Kim, I.K. Somg, J. Mol. Catal. A 246 (2006) 43.
[32] B. Pawelec, S. Damyanova, K. Arishtirova, J.L.G. Fierro, L. Petrov, Appl. Catal. A 323 (2007) 188.
[33] K. Asami, X. Li, K. Fujimoto, Y. Koyama, A. Sakurama, N. Kometani, Y. Yonezawa, Catal. Today 84 (2003) 27.
[34] V.I. Itin, Yu.S. Naiborodenko, Self-propagating High-Temperature Synthesis of Intermetallic Compounds, TSU, Tomsk, 1989.
[35] J.-W. Ren, A.-D. Shan, J.-L. Liu, J.-B. Zhang, H.-W. Song, Trans. Nonferrous Met. Soc. China 17 (2007) 69.
[36] A.N. Didenko, Yu.P. Sharkeev, E.V. Kozlov, A.I. Ryabchikov, Effects of Long-Range Action in Ion Implanted Metal Materials, INTL, Tomsk, 2004.
[37] L.A. Arkatova, T.S. Kharlamova, L.V. Galaktionova, L.N. Kurina, V.N. Belousova, Yu.S. Naiborodenko, N.G. Kasatsky, N.N. Golobokov, Russ. J. Phys. Chem. A 80 (2006) 1231.
[38] L.A. Arkatova, L.N. Kurina, L.V. Galaktionova, Russ. J. Phys. Chem. A 83 (4) (2009) 624.
[39] L.A. Arkatova, L.N. Kurina, Russ. J. Phys. Chem. A 84 (1) (2010) 19.
[40] L.A. Arkatova, Russ. J. Phys. Chem. A 84 (4) (2010) 566.
[41] L.A. Arkatova, Catal. Today 157 (2010) 170.
[42] A.G. Nikolaev, E.M. Oks, K.P. Savkin, G.Yu. Yushkov, I Brown, R. MacGill, Patent RU 48105 U1, 2005.
[43] I.G. Brown, Rev. Sci. Instrum. 65 (1994) 3061.
[44] N.P. Lyakishev, Phase Diagrams of Double Metal Systems, Mashinostroenie, Moscow, 1996.
[45] K. Arishtirova, B. Pavelec, R. Nikilov, J.L.G. Fierro, S. Damyanova, React. Kinet. Catal. Lett. 91 (2) (2007) 241.
[46] J.M. Rynkowski, T. Paryjczak, M. Lenik, M. Farbotko, J. Goralski, J. Chem. Soc. Faraday Trans. 91 (19) (1995) 3481.
[47] M.C.J. Bradford, M.A. Vannice, Appl. Catal. A. 142 (1996) 73.
[48] Y.-G. Chen, K. Tomishige, K. Fujimoto, Appl. Catal. A 161 (1997) 11.
[49] J.W. Snoeck, G.F. Froment, M. Fowles, J. Catal. 169 (1) (1997) 240.